Abbreviated MRI Protocols for the Abdomen

Rodrigo Canellas, MD
Andrew B. Rosenkrantz, MD
Bachir Taouli, MD
Evis Sala, MD, PhD
Sanjay Saini, MD
Ivan Pedrosa, MD, PhD
Zhen J. Wang, MD
Dushyant V. Sahani, MD

Technical advances in MRI have improved image quality and have led to expanding clinical indications for its use. However, long examination and interpretation times, as well as higher costs, still represent barriers to use of MRI. Abbreviated MRI protocols have emerged as an alternative to standard MRI protocols. These abbreviated MRI protocols seek to reduce longer MRI protocols by eliminating unnecessary or redundant sequences that negatively affect cost, MRI table time, patient comfort, image quality, and image interpretation time. However, the diagnostic information is generally not compromised. Abbreviated MRI protocols have already been used successfully for hepatocellular carcinoma screening, for prostate cancer detection, and for screening for nonalcoholic fatty liver disease as well as monitoring patients with this disease. It has been reported that image acquisition time and costs can be considerably reduced with abbreviated MRI protocols, compared with standard MRI protocols, while maintaining a similar sensitivity and accuracy. Nevertheless, multiple applications still need to be explored in the abdomen and pelvis (eg, surveillance of metastases to the liver; follow-up of cystic pancreatic lesions, adrenal incidentalomas, and small renal masses; evaluation of ovarian cysts in postmenopausal women; staging of cervical and uterine corpus neoplasms; evaluation of müllerian duct anomalies). This article describes some successful applications of abbreviated MRI protocols, demonstrates how they can help in improving the MRI workflow, and explores potential future directions.

Abbreviations: FSE = fast spin echo, HCC = hepatocellular carcinoma, MRCP = MR cholangiopancreatography, PI-RADS = Prostate Imaging Reporting and Data System, SSFSE = single-shot fast spin echo, 3D = three-dimensional, 2D = two-dimensional

RadioGraphics 2019; 39:744–758

https://doi.org/10.1148/rg.2019180123

Content Codes: GI GU MR OI

From the Department of Radiology, Massachusetts General Hospital, 55 Fruit St, White 270, Boston, MA 02114 (R.C., S.S., D.V.S.); Department of Radiology, NYU Langone Health, New York, NY (A.B.R.); Department of Radiology, Mount Sinai Hospital, New York, NY (B.T.); Department of Radiology, University of Cambridge, Cambridge, England (E.S.); Department of Radiology, University of Texas Southwestern Medical Center, Dallas, Tex (I.P.); and Department of Radiology, UCSF Medical Center, San Francisco, Calif (Z.J.W.). Presented as an education exhibit at the 2017 RSNA Annual Meeting. Received April 7, 2018; revision requested May 31 and received June 28; accepted July 13. For this journal-based SA-CME activity, the authors B.T. and D.V.S. have provided disclosures (see end of article); all other authors, the editor, and the reviewers have disclosed no relevant relationships. **Address correspondence to** D.V.S. (e-mail: *DSAHANI@mgh.harvard.edu*).

SA-CME LEARNING OBJECTIVES

After completing this journal-based SA-CME activity, participants will be able to:

- Explain the concept behind abbreviated MRI protocols.
- Describe how abbreviated MRI protocols can help improve the MRI workflow.
- Discuss strategies to design abbreviated MRI protocols for the abdomen and pelvis.

See rsna.org/learning-center-rg.

Introduction

During the past 3 decades, MRI has experienced rapid growth in the clinical indications for its use. Important technologic advances in MRI, including improvements in data acquisition, image reconstruction, postprocessing denoising, and artifact reduction have contributed to the growth of clinical applications (1–4). These advances have established MRI as among the most powerful tools for imaging. However, a tendency exists for such newly developed sequences and other techniques to continually be added to earlier MRI protocols, rather than to replace existing sequences, thereby leading to progressively longer imaging times and associated workflow challenges.

TEACHING POINTS

- The increasing emphasis on patient-centered care in radiology is affecting the way that radiologists think about and design their MRI protocols.
- The development of efficient and precise MRI protocols aligns with the needs of patients, referring physicians, and radiologists alike and represents a growing trend across radiology practices.
- Investigators have demonstrated that identifying possible inefficiencies and implementing change can cause substantial improvement in patient centricity (patient centeredness) and workflow efficiency in MRI departments.
- Utilization of abbreviated MRI protocols represents an opportunity to improve the MRI workflow, reduce costs, and meet increasing clinical demands for MRI.
- The MRI workflow for radiologists is also likely to improve because there would be fewer sequences to review and interpret.

On the other hand, the increasing emphasis on patient-centered care in radiology is affecting the way that radiologists think about and design their MRI protocols (5). Instead of applying long time-consuming comprehensive protocols for a specific organ, use of short focused protocols to answer a targeted clinical question may add value to patient care and improve the patient experience.

Moreover, shorter MRI protocols help to expand patient access and meet the growing clinical demands. Therefore, the development of efficient and precise MRI protocols aligns with the needs of patients, referring physicians, and radiologists alike and represents a growing trend across radiology practices. The underlying rationale behind these new abbreviated MRI protocols is to reduce the number of sequences, compared with standard MRI protocols, without compromising diagnostic information, so as to yield faster overall imaging times and, ultimately, to optimize resource utilization. The purpose of this article is to demonstrate applications of abbreviated MRI protocols and to explore potential future directions.

Optimizing MRI Logistics

The table time for an MRI examination can be divided into three intervals with different value weighting: *(a) value-added time* (activities that directly benefit patients, primarily the actual image acquisition time), *(b) business value-added time* (necessary activities that consume time but do not directly influence patient care, such as preparing or cleaning the room), and *(c) non–value-added time* (time lost without activity, such as when the imaging equipment is idle) (6). Investigators have demonstrated that identifying possible inefficiencies and implementing change can cause substantial improvement in patient centricity (patient centeredness) and workflow efficiency in MRI departments (7–9). Common causes of delay, which increases non–value-added time, include intravenous or port access issues (the most frequent source of delay), patient needs (eg, issues with paperwork), the late arrival of an interpreter, and concerns about implants or other safety issues. An online screening process before the day of the MRI examination may reduce these delays substantially (10).

For liver MRI, patient throughput and imaging volume can be increased by using automated MRI field detection at scout imaging, in combination with interleaved acquisitions with sequences that have differing sensitivities to breathing motion. Specifically, rather than the MRI system remaining idle while patients regain their breath between breath holds, the system collects data for sequences that are less affected by respiratory motion. In addition, the acquisition of diffusion-weighted and T2-weighted sequences can be done after the administration of gadoxetic acid, to use some of the wait time needed to obtain the hepatocellular phase (usually ~20 minutes) (11).

Such process improvements can play a major role in increasing key performance indicators such as the total number of MRI examinations, on-time performance, and the percentage of examinations completed within their allotted time slots. However, process improvements affect only the non–value-added time, which represents approximately 30% of the total patient stay.

Additional MRI Advances

Recently, tremendous interest has been expressed with regard to novel strategies for accelerating MR image acquisition. These strategies use a range of methods to more rapidly fill k-space, compared with conventional MRI methods. These rapid acquisition techniques represent opportunities to further decrease the imaging time and improve the efficiency of abbreviated MRI protocols (12). Examples include higher-order parallel imaging, k-space and temporal dimension acceleration, the compressed sensing technique, non-Cartesian acquisition, and simultaneous multisection imaging.

Parallel imaging is a technique that can accelerate the acquisition by allowing image recovery from the undersampled k-space. The process is accomplished through phased-array coils, which contain multiple independent receiver channels (13,14). In partial Fourier imaging, the k-space is not fully sampled, and a contiguous fraction is not acquired. Image recovery relies on exploiting conjugate symmetry of k-space or on slowly varying the phase (15,16).

The technique of k-space and temporal dimension acceleration is used for dynamic applications that collect MRI data in the k-space and temporal dimension domain. This domain enables image recovery at high acceleration rates. Methods of k-space and temporal acceleration can achieve higher acceleration rates, compared with parallel MR images, at a cost of temporal blurring (17).

The compressed sensing technique exploits image structure—in the form of sparsity—to facilitate recovery from highly undersampled data. Compared with k-space and temporal dimension acceleration methods, compressed sensing methods generate images with less temporal blurring and with a suppressed undersampling artifact (18,19).

In non-Cartesian acquisition, the acquired samples are not restricted to a Cartesian grid (eg, radial or spiral). These trajectories can reduce the acquisition time by enabling more efficient coverage of k-space and are more robust with respect to motion artifacts (20,21). Simultaneous multisection imaging allows simultaneous excitation and acquisition of multiple sections, improving the signal-to-noise ratio and reducing acquisition time. By applying a section-specific phase gradient in k-space, the superimposed sections can be shifted with respect to one another to further improve the separation process (22).

Since its clinical implementation, diffusion-weighted MRI had been used largely as a tool to complement conventional MRI sequences. However, diffusion-weighted MRI was associated with relatively low spatial resolution that hindered anatomic assessment of these images. Recent advances in imaging equipment hardware and postprocessing techniques have helped improve the image quality of diffusion-weighted MR images (23,24).

Currently, diffusion-weighted MRI is emerging as a critical pulse sequence in abbreviated MRI protocols owing to *(a)* its capacity to serve as an alternative to contrast agent–enhanced T1-weighted MR images in multiple clinical scenarios (eg, characterization of liver, renal, and prostate lesions) and *(b)* the potential of diffusion-weighted MRI with a low *b* value to replace fast spin-echo (FSE) T2-weighted fat-suppressed MR images that have relatively prolonged acquisition times (25–28).

Three-dimensional (3D) T2-weighted pulse sequences have also recently become clinically available. The generated volumetric dataset can potentially replace the typical acquisition of two-dimensional (2D) T2-weighted MR images in multiple separate planes. This 3D T2-weighted technique may also serve to shorten abbreviated MRI protocols, especially those used for the female pelvis and male pelvis, in which the acquisition of T2-weighted MR images in multiple planes is standard (29).

Health Care Economics

Utilization of abbreviated MRI protocols represents an opportunity to improve the MRI workflow, reduce costs, and meet increasing clinical demands for MRI. In comparison to standard protocols, investigators using abbreviated MRI protocols have demonstrated that MR image acquisition time can be reduced to less than half (30,31). Shorter MRI protocols may also improve image quality through reduction of motion artifacts. Although the payment per MRI examination may decrease, this decrease may not negatively affect overall revenue, owing to an increase in available MRI slots and the overall capacity of the MRI equipment. For hepatocellular carcinoma (HCC) screening, investigators have demonstrated that an abbreviated MRI protocol consisting of only two sequences had a diagnostic performance similar to that of the standard MRI protocol (31). By using this highly shortened MRI protocol, three patients could potentially undergo HCC screening in the place of a single standard contrast-enhanced MRI time slot.

The MRI workflow for radiologists is also likely to improve because there would be fewer sequences to review and interpret (32). Furthermore, a faster report turnaround time can be achieved, as well as a shorter length of hospitalization for inpatients, whose discharge is sometimes delayed owing to pending imaging studies.

Current Clinical Applications of Abbreviated MRI Protocols and Future Directions

Liver

Screening for and Surveillance of HCC.—For patients at risk for HCC, the American Association for the Study of Liver Diseases recommends semiannual surveillance with US and determination of the α-fetoprotein level (optional) (33). Although this strategy has been shown to decrease mortality from HCC by 37% (34), many centers in the United States adopt contrast-enhanced MRI or contrast-enhanced CT owing to their greater sensitivity, compared with that of US (35–37). Nevertheless, the high cost of MRI limits its routine use, and different strategies have been proposed to overcome this limitation.

In a dual-center retrospective study with 298 patients, Marks et al (38) assessed whether use of a virtual abbreviated MRI protocol (including only a T2-weighted single-shot fast spin-echo

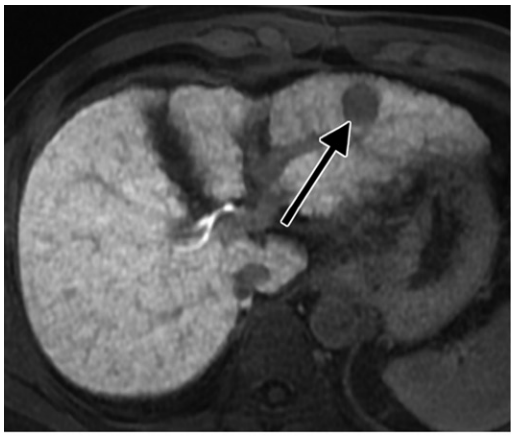

Figure 1. Cirrhosis in a 44-year-old man. **(a)** Axial contrast-enhanced T1-weighted hepatobiliary phase MR image obtained at 20 minutes after gadoxetic acid injection shows a 2.7-cm HCC (arrow). **(b, c)** Axial diffusion-weighted MR image **(b)** and apparent diffusion coefficient map **(c)** show diffusion restriction within the lesion (arrow).

a.

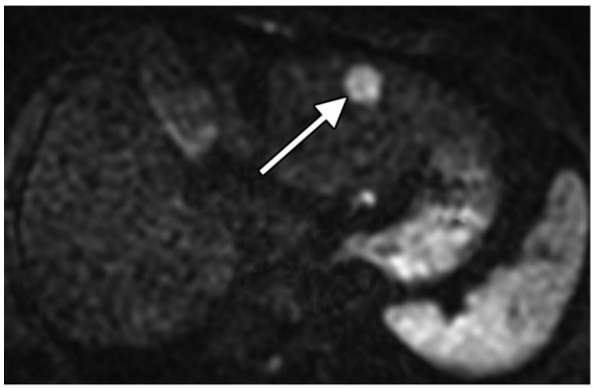

b.

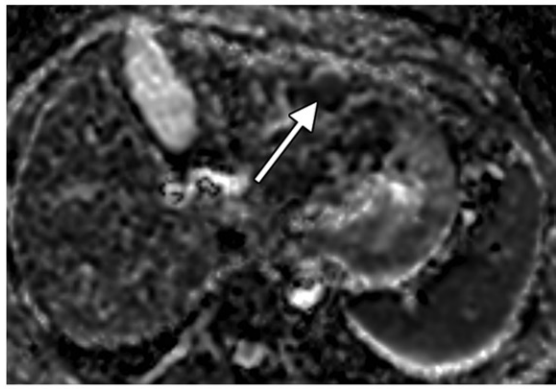

c.

[SSFSE] sequence and a contrast-enhanced T1-weighted hepatobiliary phase sequence after gadoxetic acid injection) extracted from a full contrast-enhanced MRI protocol could provide adequate sensitivity and negative predictive values for HCC surveillance (Fig 1). Marks et al (38) reported a mean per-patient sensitivity and negative predictive value of 82.6% (95% confidence interval: 70.9%, 90.7%) and 93.2% (95% confidence interval: 90.0%, 95.6%), respectively. When diffusion-weighted MRI was added to these sequences, no significant improvement was detected. Marks et al (38) concluded that their abbreviated MRI protocol may be an acceptable lower-cost alternative to the standard contrast-enhanced MRI protocol.

In the results of a retrospective single-center study with 174 patients with and without HCC, Besa et al (39) demonstrated that a virtual abbreviated MRI protocol extracted from a full contrast-enhanced MRI examination (abbreviated protocol: contrast-enhanced T1-weighted hepatobiliary phase after gadoxetic acid injection, diffusion-weighted MRI, T1-weighted in-phase and out-of-phase, and T2-weighted FSE sequences) yielded a per-patient sensitivity of 80.6% (95% confidence interval: 70.7%, 87.8%) and a negative predictive value of 90.0% (95% confidence interval: 84.0%, 93.9%), in comparison with the full MRI protocol (sensitivity of 90.3% and negative predictive value of 94.9%). Moreover, the estimated cost reduction of the abbreviated MRI protocol ranged between 30.7% and 49.0% below the standard MRI cost. Besa et al (39) concluded that their protocol also had a clinically acceptable sensitivity and negative predictive value for HCC screening, with decreased costs.

In the findings from a retrospective study of 156 patients with use of an extracellular gadolinium-based contrast agent, Lee et al (40) reported strong agreement between an abbreviated MRI protocol (including only nonenhanced and dynamic contrast-enhanced T1-weighted images) and the standard contrast-enhanced MRI protocol. With both protocols, 95% of lesions were correctly characterized by using the Liver Imaging Reporting and Data System (LI-RADS) categorization. Lee et al (40) concluded that their HCC screening protocol had a detection and characterization performance similar to the standard MRI protocol and was more cost-effective.

Detection of Metastases to the Liver.—Metastatic disease in the liver is the most common cause of malignant liver lesions worldwide. The

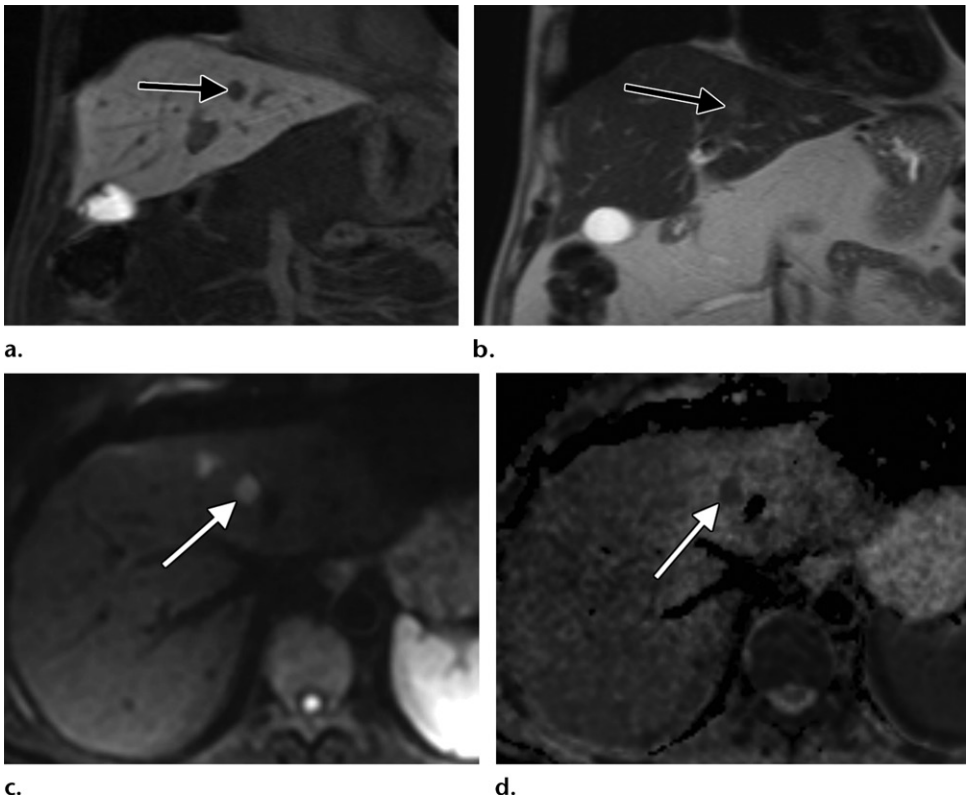

Figure 2. Colorectal cancer metastatic to the liver in a 51-year-old man. **(a, b)** Coronal T1-weighted hepatobiliary phase MR image obtained at 20 minutes after gadoxetic acid administration **(a)** and coronal SSFSE T2-weighted MR image **(b)** show a 1.4-cm metastatic lesion (arrow) in the left liver lobe. **(c, d)** Axial diffusion-weighted MR image (b = 800 sec/mm^2) **(c)** and apparent diffusion coefficient map **(d)** show the restricted diffusion within the lesion (arrow).

choice of appropriate therapy requires the accurate and clinically appropriate staging of metastatic liver disease (41).

Excellent results have been reported for use of abbreviated MRI protocols for the detection and characterization of metastases to the liver. In a study of 71 patients who underwent MRI to search for metastases to the liver, Barabasch et al (42) investigated whether a nonenhanced protocol consisting of T2-weighted FSE, diffusion-weighted MRI, and T1-weighted in-phase and opposed-phase sequences was appropriate to detect and classify liver lesions. Compared with the standard MRI protocol with gadoxetic acid administration, Barabasch et al (42) reported high sensitivity (98.2% and 100% for two readers) for the detection of liver lesions and high positive predictive values (92% and 88%) for characterization. An acquisition time of 10.3 minutes and a reading time of between 42 and 72 seconds were reported for the abbreviated MRI protocol.

In a retrospective study of 43 patients with pathologically proven colorectal cancer metastases to the liver, Canellas et al (43) evaluated the lesion detection performance of a protocol consisting of T2-weighted SSFSE, diffusion-weighted MRI, and T1-weighted hepatobiliary phase sequences at 20 minutes after gadoxetic acid administration (Fig 2). Excellent inter- and intraobserver agreement (>0.85) and high sensitivity (>90%) were reported for two readers. The acquisition time was estimated at around 15 minutes. Canellas et al (43) concluded that their abbreviated MRI protocol is a cost-effective alternative to the standard contrast-enhanced MRI protocol for detection and follow-up of metastases to the liver from colorectal cancer.

Assessment of Liver Fat and Fibrosis.—Nonalcoholic fatty liver disease is currently the main cause of chronic liver disease in the developed countries of the world. Although percutaneous biopsy is the reference standard method to estimate liver fat, MRI has been successfully used as a noninvasive biomarker to assess for liver fibrosis and to quantify liver fat (44).

In a prospective study with 25 patients, Cunha et al (45) used an abbreviated MRI protocol to analyze quantitative imaging features and assessed its use during treatment of patients with obesity and nonalcoholic fatty liver disease. All patients were referred for MRI evaluation

Table 1: Sequences for the Standard MRI Protocol and Various Abbreviated MRI Protocols for Liver Diseases

Standard MRI protocol: HCC screening
Coronal SSFSE T2 weighted
Axial FSE T2 weighted with fat saturation
Axial diffusion weighted
Axial in-phase and out-of-phase T1 weighted
Axial nonenhanced T1 weighted with fat saturation
Axial contrast-enhanced T1 weighted with fat saturation (arterial, portal, and delayed phases)
Coronal contrast-enhanced T1 weighted with fat saturation (delayed phase)
Axial contrast-enhanced T1 weighted with fat saturation, hepatobiliary phase, at 10 and 20 min*
Coronal contrast-enhanced T1 weighted with fat saturation, hepatobiliary phase, at 10 and 20 min*
Abbreviated MRI protocol: HCC screening
Axial SSFSE T2 weighted
Axial contrast-enhanced T1 weighted with fat saturation, hepatobiliary phase, at 20 min
Abbreviated MRI protocol: HCC screening
Axial diffusion weighted
Axial contrast-enhanced T1 weighted with fat saturation, hepatobiliary phase, at 20 min
Abbreviated MRI protocol: HCC screening
Axial nonenhanced T1 weighted with fat saturation
Axial contrast-enhanced T1 weighted with fat saturation (arterial, portal, and delayed phases)
Nonalcoholic fatty liver disease surveillance
Axial and coronal SSFSE T2 weighted
Fast 3D spoiled gradient echo†
2D gradient-echo MR elastography
Abbreviated MRI protocol for metastases to the liver
Axial FSE T2 weighted with fat saturation
Axial diffusion weighted
Axial in-phase and out-of-phase T1 weighted
Abbreviated MRI protocol for colorectal cancer metastases to the liver
Coronal SSFSE T2 weighted
Axial diffusion weighted
Axial and coronal contrast-enhanced T1 weighted with fat saturation, hepatobiliary phase, at 20 min

*These sequences are used only after gadoxetic acid injection; all of the other sequences are common after extracellular contrast agent injection and gadoxetic acid injection.
†IDEAL IQ software (GE Healthcare, Waukesha, Wis).

during the course of a physical activity program for overweight and obesity treatment and underwent quantitative analysis of liver fat and iron content, liver stiffness, and visceral adipose tissue. The abbreviated MRI protocol took less than 10 minutes to complete. Cunha et al (45) concluded that it represents a feasible, less costly, and accessible option for screening and monitoring patients with obesity, nonalcoholic fatty liver disease, and metabolic syndrome. Although no data exist with regard to use of abbreviated MRI protocols for iron overload, a reasonable protocol would focus on only the assessment of iron overload, without use of all of the other conventional sequences within a full contrast-enhanced MRI protocol. Nevertheless, the full MRI protocol would be used for HCC screening in the same population, as warranted.

Table 1 summarizes the sequences for the standard MRI protocol and various abbreviated MRI protocols for liver diseases.

Pancreas: Cystic Pancreatic Lesions

The prevalence of incidentally detected pancreatic cystic lesions has increased because of advances in diagnostic imaging. This increase is expected to yield increases in follow-up imaging and associated costs (46). Although contrast-enhanced CT is cheaper than the standard contrast-enhanced MRI examination, CT is not considered the ideal imaging modality to characterize small cystic lesions, given its lower contrast resolution, or to follow these patients, given the radiation exposure associated with CT (47). In this sense, abbreviated MRI protocols may represent a good alternative to follow the patients.

To our knowledge, Macari et al (48) were the first to question the need to administer a gadolinium-based contrast agent for the evaluation of patients with pancreatic cysts who are undergoing follow-up imaging. In the results of a preliminary retrospective study of 56 patients with pancreatic cysts, the treatment recommendations after interpretation of MRI performed without and with administration of a gadolinium-based contrast agent were concordant in more than 95% of patients. Upon review of five cases in which there were discrepancies in the recommendation, the consensus was that there was nothing on the gadolinium-enhanced images that would lead to a different recommendation.

Nougaret et al (49) reported their follow-up data after using an MRI protocol without and with administration of a contrast agent in 301 patients and 1174 cysts. The morphologic structure and size of the cyst changed at follow-up imaging in only 35 patients (12%), corresponding to 3% of all of the cysts. None of the lesions that were smaller than 2 cm developed malignancy. Evaluation of the contrast-enhanced MRI component of the protocol led to the conclusion

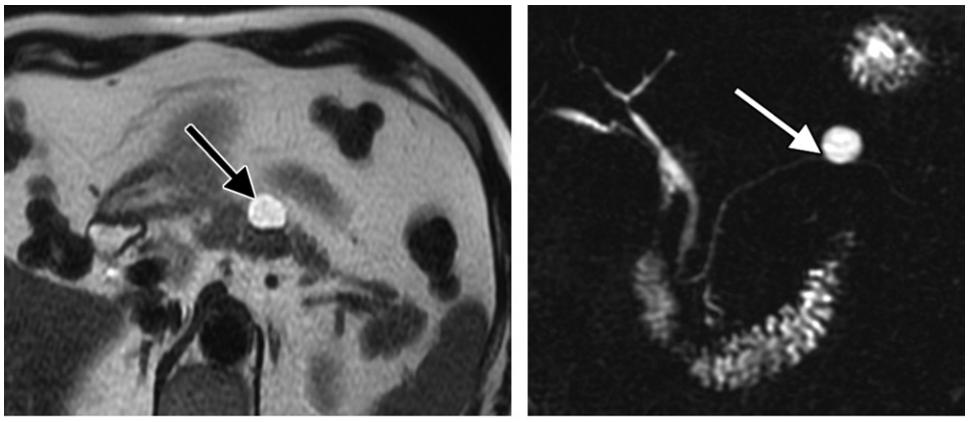

a. b.

Figure 3. Pancreatic cystic lesion found at US in a 64-year-old woman. **(a)** Axial SSFSE T2-weighted MR image shows a 2.0-cm cystic lesion (arrow) in the pancreatic body. **(b)** Coronal 2D single-shot MRCP image shows the lesion (arrow) adjacent to the main pancreatic duct; the lesion is likely an intraductal papillary mucinous neoplasm.

that the administration of a contrast agent did not provide additional information. The size of the cyst at diagnosis was the only predictor of growth or development of an internal nodule.

The American College of Radiology Incidental Findings Committee updated their recommendations for the follow-up of incidental pancreatic cysts in 2017 (50). On the basis of their recommendations, in most clinical scenarios, patients younger than 80 years old with cysts smaller than 1.5 cm require follow-up imaging for up to 10 years after the initial diagnosis.

Pedrosa (51) proposed an optimized abbreviated MRI protocol consisting of SSFSE T2-weighted (axial and coronal), 2D and 3D single-shot MR cholangiopancreatography (MRCP) (Fig 3), and 3D Dixon T1-weighted spoiled gradient-echo sequences to follow pancreatic cystic lesions. This MRI protocol could be used in subsequent visits after patients have undergone an initial evaluation with standard contrast-enhanced MRI and MRCP. The nonenhanced MRI protocol proposed by Pedrosa (51) included high-spatial-resolution 3D MRI acquisitions. Diffusion-weighted sequences can be added if a contrast agent is not administered, although the utility of diffusion-weighted MRI to predict progression of pancreatic cysts and/or development of pancreatic cancer has not been proven. Table 2 shows the sequences included in both the standard and abbreviated MRI protocols for follow-up of cystic pancreatic lesions.

Technical developments are on the way to facilitate the replacement of standard respiratory-triggered 3D FSE acquisitions, typically requiring 5–7 minutes; these standard acquisitions will be replaced with breath-hold acquisitions with superior image quality (ie, elimination of ghosting caused by respiratory motion). Such techniques include 3D FSE MRCP acquisitions with compressed sensing and acquisitions with 3D gradient- and spin-echo sequences. The incorporation of such sequences allows for an abbreviated MRI protocol with a total examination time of about 5 minutes. Furthermore, the cost savings of not administering a gadolinium-based contrast agent for follow-up of pancreatic cysts in the U.S.

Table 2: Sequences for the Standard and Abbreviated MRI Protocols for Cystic Pancreatic Lesions

Standard MRI protocol
Coronal SSFSE T2 weighted
Axial FSE T2 weighted with fat saturation
Axial diffusion weighted
Axial in-phase and out-of-phase T1 weighted
Axial nonenhanced T1 weighted with fat saturation
Axial contrast-enhanced T1 weighted with fat saturation (arterial, portal, and delayed phases)
Coronal contrast-enhanced T1 weighted with fat saturation (delayed phase)
Coronal 2D single-shot MRCP
Coronal 3D single-shot MRCP
Abbreviated MRI protocol
Axial SSFSE T2 weighted
Coronal SSFSE T2 weighted
Coronal 2D single-shot MRCP
Coronal 3D single-shot MRCP*
3D T1-weighted spoiled gradient echo

*Breath-hold 3D FSE MRCP acquisitions with compressed sensing and 3D gradient- and spin-echo sequences can shorten the examination time substantially. Dixon acquisitions with reconstruction of water, fat, in-phase, and opposed-phase images are preferred, because they may help differentiate fat infiltration from true parenchymal lesions (eg, adenocarcinoma).

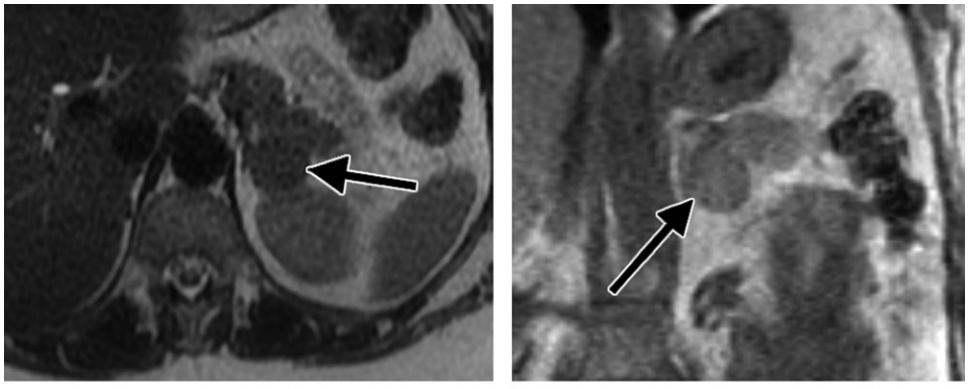

a. b.

c.

Figure 4. Adrenal nodule found at contrast-enhanced CT of the abdomen in a 74-year-old woman. **(a, b)** Axial SSFSE T2-weighted **(a)** and coronal in-phase T1-weighted **(b)** MR images show a 2.4-cm left adrenal nodule (arrow). **(c)** Coronal out-of-phase MR image shows decreased signal intensity in the lesion (arrow), a finding consistent with a lipid-containing adenoma.

population between 40 and 84 years old would be enormous (ie, probably on the order of several billion dollars), considering a reported prevalence of 2.5% and the average number of follow-up MRI examinations performed per patient during a 10-year follow-up interval (52).

Adrenal Glands: Adrenal Incidentalomas

The frequency of adrenal incidentalomas at radiologic examinations is estimated to be 3% in patients younger than 50 years old and 10% in patients older than 50 years (53). Guidelines primarily recommend the use of nonenhanced CT to characterize these lesions. If the attenuation is less than or equal to 10 HU and the mass is homogeneous at nonenhanced CT, then a benign cause is presumed, and no further imaging is required. When the mass is indeterminate (>10 HU), measures 4 cm or less, and is nonfunctioning, interval follow-up imaging every 6–12 months is recommended (54). Therefore, for indeterminate lesions, abbreviated MRI protocols including T1-weighted in-phase and out-of-phase (to detect lipid, proteinaceous, and/or hemorrhagic components), SSFSE T2-weighted (to detect cystic components), and diffusion-weighted (to detect hypercellular components) sequences could represent an alternative to the standard contrast-enhanced MRI protocol and provide a radiation-free alternative to contrast-enhanced CT (Fig 4).

Kidneys: Active Surveillance for Small Renal Masses

The detection of small renal masses (≤4 cm) has increased in recent decades (55). The findings from prospective and retrospective studies have shown very low progression rates for these tumors (<2%), even when they are malignant. In this regard, active surveillance has emerged as a good option for suboptimal surgical candidates and for those not requiring surgery. For these patients, the growth rate is often used to guide treatment selection during surveillance of a small renal mass (56). Therefore, an abbreviated MRI protocol consisting of T1-weighted in-phase and out-of-phase, SSFSE T2-weighted, and diffusion-weighted sequences (similar to the MRI protocol for adrenal incidentalomas) could also represent an alternative to the standard contrast-enhanced MRI protocol and provide a radiation-free alternative to contrast-enhanced CT (Fig 5).

Male Pelvis: Prostate Cancer

Multiparametric MRI is considered the modality of choice to evaluate patients who are suspected of having prostate cancer (57). Prostate MRI has experienced enormous growth in use in recent years (58), given its role in guiding prostate biopsy to increase the detection of clinically important cancer. However, the generally long imaging times of multiparametric MRI have contributed to a strong interest in reducing the length of multiparametric MRI protocols. Various strategies have been explored for achieving such a reduction, in part reflecting the distinct nature of the examination when performed in a prebiopsy setting primarily for the purpose

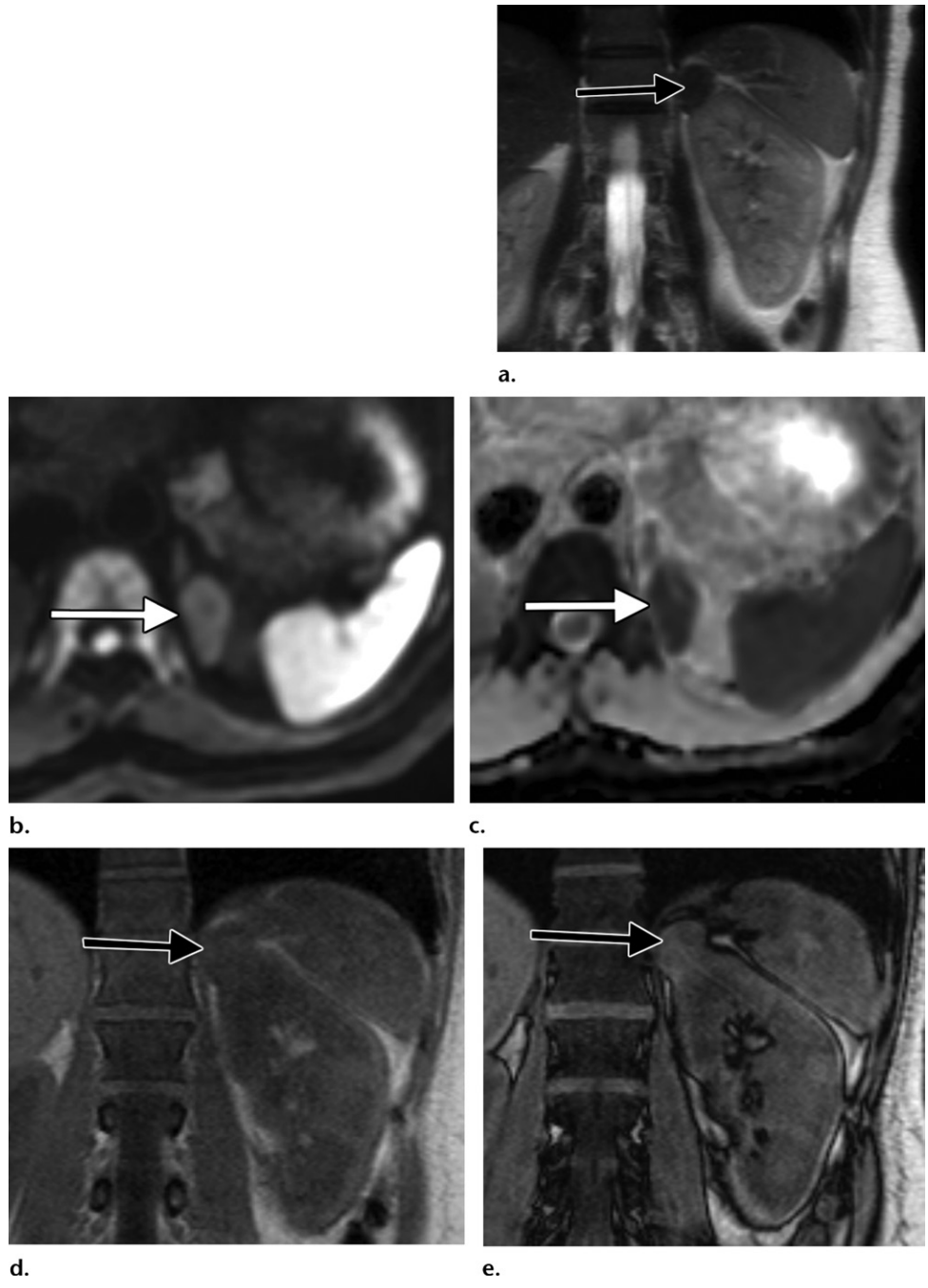

Figure 5. Active surveillance of a left renal mass found at chest CT in a 68-year-old man. **(a–c)** Coronal SSFSE T2-weighted MR image **(a)**, axial diffusion-weighted MR image **(b)**, and axial apparent diffusion coefficient map **(c)** show a partially exophytic 2.3-cm mass (arrow) in the upper pole of the left kidney, a finding that is concerning for renal malignancy or a lipid-poor angiomyolipoma. **(d, e)** Coronal in-phase **(d)** and out-of-phase **(e)** T1-weighted MR images show no fat component in the lesion (arrow). The lesion has remained stable since the initial CT examination.

of identifying biopsy targets, rather than in a setting of preoperative staging of known cancer. These strategies include *(a)* use of external coils, rather than endorectal coils; *(b)* the acquisition of only axial FSE T2-weighted or 3D T2-weighted MR images of the prostate, rather than FSE T2-weighted MR images of the prostate in three separate planes; and *(c)* the elimination of whole-pelvis imaging (59).

An additional protocol modification to further reduce the length of multiparametric MRI protocols is to eliminate use of dynamic contrast-enhanced MRI (Fig 6). In a prospective study with 82 patients, Stanzione et al (60) assessed the diagnostic accuracy of a biparametric (T2-weighted and diffusion-weighted MRI) 3-T MRI protocol in a biopsy-naïve population of patients in whom there was a clinical suspicion for prostate cancer.

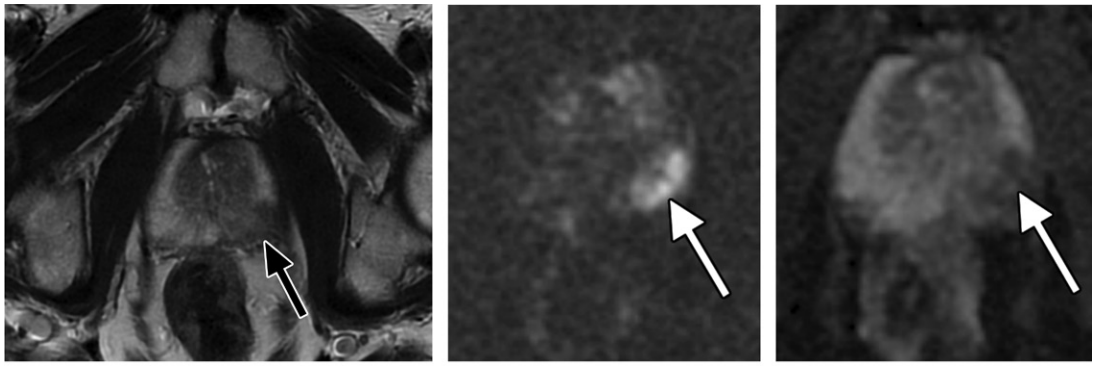

a. b. c.

Figure 6. Biopsy-proven prostate cancer in a 68-year-old man. **(a)** Axial T2-weighted MR image obtained with the PROPELLER (periodically rotated overlapping parallel lines with enhanced reconstruction) sequence shows a 19-mm hypointense lesion (arrow) in the left peripheral zone, extending from the apex of the prostate gland to mid gland. The indistinctness of the capsule is suggestive of an extraprostatic extension. **(b, c)** Axial diffusion-weighted MR image (b = 2000 sec/mm^2) **(b)** and apparent diffusion coefficient map **(c)** show associated restricted diffusion (Prostate Imaging Reporting and Data System [PI-RADS] category 5) (arrow). (Case courtesy of Amirkasra Mojtahed, MD, Massachusetts General Hospital, Boston, Mass.)

Table 3: Sequences for the Standard and Biparametric Abbreviated MRI Protocols for the Prostate Gland

Standard MRI protocol
Axial, coronal, and sagittal FSE T2 weighted
Axial diffusion weighted
Axial nonenhanced FSE T1 weighted with fat saturation
Axial dynamic contrast-enhanced T1 weighted with fat saturation
Biparametric abbreviated MRI protocol
Axial FSE T2 weighted
Axial diffusion weighted

Stanzione et al (60) reported a similar performance of the biparametric (≈17 min) and the multiparametric (≈24 min) MRI protocols in the detection of clinically important prostate cancer, with values for the area under the curve of 0.91 and 0.93, respectively.

Kuhl et al (61) used a faster biparametric MRI protocol (≈9 min) on 3-T imaging equipment to retrospectively assess the lesion detection performance of the protocol in 542 men. An accuracy of 89.1% (483/542) and an interobserver agreement of $\kappa = 0.81$ were reported for the abbreviated MRI protocol.

In the findings from a prospective study of 52 patients, Weiss et al (30) also achieved excellent results with the fastest biparametric MRI protocol reported so far (≈5 min). An accelerated diffusion-weighted MRI sequence with a simultaneous multisection technique was implemented and shortened the standard diffusion-weighted MRI sequence by more than 2 minutes. Weiss et al (30) reported excellent diagnostic performance, with a sensitivity and specificity of 100% for two readers.

Note that controversy currently exists with regard to the value of dynamic contrast-enhanced MRI in prostate cancer detection and characterization, and PI-RADS version 2 recommends that dynamic contrast-enhanced sequences be included in all multiparametric MRI examinations. Although PI-RADS version 2 assigns to dynamic contrast-enhanced MRI a relatively minor role in determining overall assessment categories for detected lesions, the system does note that dynamic contrast-enhanced MRI may have a role in initial lesion detection. For example, Greer et al (62) reported meaningful improvements in prostate cancer detection for PI-RADS categories 2, 3, and 4 when incorporating dynamic contrast-enhanced MRI.

Table 3 summarizes the sequences for the standard MRI protocol and the biparametric abbreviated MRI protocol for the prostate gland.

Female Pelvis

Ovaries.—The evaluation of incidentally detected ovarian cysts in postmenopausal women represents an opportunity to use abbreviated MRI protocols in the female pelvis. Guidelines recommend that postmenopausal ovarian cysts larger than 10 mm should be initially assessed by measuring the serum level of the ovarian cancer antigen CA-125 and by performing a transvaginal US examination. MRI is recommended as a second-line imaging modality in cases in which the US findings are inconclusive (63,64). An abbreviated MRI protocol consisting of nonenhanced T1-weighted (axial plane; to detect proteinaceous or hemorrhagic components), SSFSE T2-weighted (coronal

Figure 7. Right adnexal lesion found at contrast-enhanced CT in a 58-year-old woman. **(a)** Coronal FSE T2-weighted MR image shows a 4.7-cm cyst (arrow) in the right ovary. **(b, c)** Axial nonenhanced T1-weighted **(b)** and diffusion-weighted **(c)** MR images do not depict hemorrhagic or solid components in the lesion (arrow).

and axial planes; to detect and evaluate septa), and diffusion-weighted (axial plane; to detect solid components) sequences may represent an alternative to US in evaluating these cysts (Fig 7). The abbreviated MRI protocol can eliminate the problem of operator dependence and may provide better or similar accuracy in the characterization of ovarian cystic lesions.

Neoplasms of the Cervix and Uterine Corpus.— Although MRI is not officially incorporated into the staging system of the International Federation of Gynecology and Obstetrics (FIGO), MRI has been widely used for diagnosis, staging, and planning treatment of cervical and uterine cancer (65,66). It has also been demonstrated that contrast-enhanced MR images do not improve the accuracy of staging, compared with nonenhanced T2-weighted MR images and diffusion-weighted MR images for both types of neoplasms (67–70). Therefore, a suggested abbreviated MRI protocol for cervical cancer staging would include an axial oblique high-spatial-resolution FSE T2-weighted sequence used perpendicular to the cervical canal (which provides a more accurate assessment of stromal involvement and parametrial invasion), an FSE T2-weighted sequence (axial and sagittal planes), and a diffusion-weighted sequence (axial and axial oblique planes to match the T2-weighted sequences) (Fig 8). A similar protocol could be used for uterine cancer; however, the oblique sequences (high-spatial-resolution FSE T2-weighted and diffusion-weighted MRI, the latter needed for analysis of the depth of myometrial invasion) would be acquired perpendicular to the uterine body.

Table 4 summarizes proposed abbreviated MRI protocols for surveillance of adrenal incidentalomas and small renal masses, surveillance of postmenopausal ovarian cysts, and staging of cervical and uterine cancer.

Müllerian Duct Anomalies.—MRI has been considered the reference standard imaging modality for the diagnosis of müllerian duct anomalies (71). An abbreviated MRI protocol consisting of 3D T2-weighted and nonenhanced T1-weighted (axial plane) sequences for the pelvis and coronal SSFSE T2-weighted sequences for the abdomen would provide useful information with regard to the uterine structure, the presence of blood products in the uterine cavity, and the presence of renal anomalies (Fig 9).

Limitations of Abbreviated MRI Protocols and Practical Recommendations

Given the limited data with regard to use of abbreviated MRI protocols in the abdomen, these applications should be used with caution in clinical practice. Moreover, some of the suggested abbreviated MRI protocols, although reasonable, are not yet supported by professional society guidelines and/or expert consensus opinion. However, these protocols use vast

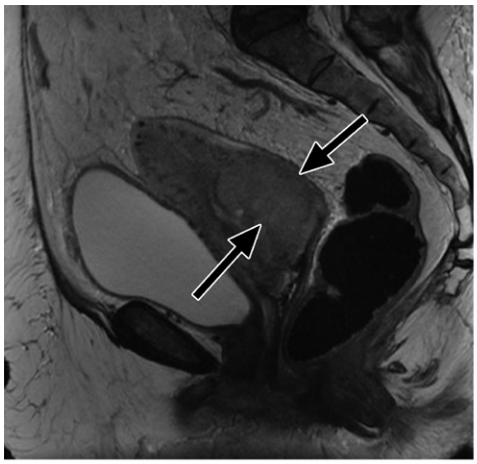

a.

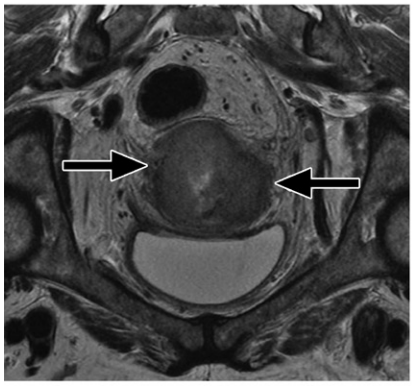

b.

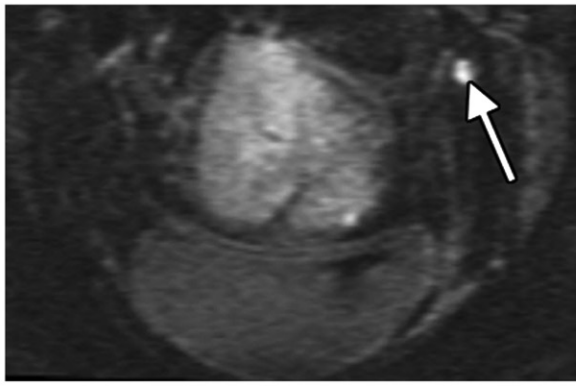

c.

Figure 8. Cervical cancer in a 77-year-old woman. **(a)** Sagittal FSE T2-weighted MR image shows a large cervical mass (arrows). **(b)** Axial oblique T2-weighted MR image shows bilateral parametrial invasion (stage IIB) (arrows). **(c)** Axial oblique diffusion-weighted MR image shows a left pelvic lymph node (arrow), a finding suspicious for metastatic disease.

Table 4: Comparison of Proposed Abbreviated MRI Protocols for Adrenal Incidentaloma and Small Renal Mass Surveillance, Postmenopausal Ovarian Cyst Surveillance, and Cervical or Uterine Cancer Staging

Adrenal Incidentaloma and Small Renal Mass Surveillance	Postmenopausal Ovarian Cyst Surveillance	Cervical or Uterine Cancer Staging
Coronal in-phase and out-of-phase T1 weighted	Axial nonenhanced T1 weighted	High-spatial-resolution FSE T2 weighted, perpendicular to the cervical canal or uterine body
3D FSE T2 weighted	3D FSE T2 weighted	3D FSE T2 weighted
Axial diffusion weighted	Axial diffusion weighted	Axial diffusion weighted

clinical experience and published research on the value of certain sequences in each organ by eliminating redundancies. We hope to encourage readers to build abbreviated MRI protocols, by using the most relevant sequences, and to start research studies to validate the use of such protocols in clinical practice.

Nevertheless, we believe that the majority of the abbreviated MRI protocols will be used as surveillance or screening tools at this preliminary stage. In the surveillance setting, a prior standard MRI protocol should be available for comparison and to help in characterizing all preexisting lesions. In the screening setting, only positive examinations with indeterminate findings will require a new examination with the standard protocol. However, radiologists should not hesitate to use the standard MRI protocol at any time when clinically indicated. Future work, including cost-effectiveness and cost-modeling analyses, should also be performed to address issues with regard to billing and reimbursement.

One approach to consider during implementation of abbreviated MRI protocols is to perform the initial examinations under supervision. In this sense, any modification of the original protocol can be evaluated in a real-time setting, and any sequence can be repeated if necessary.

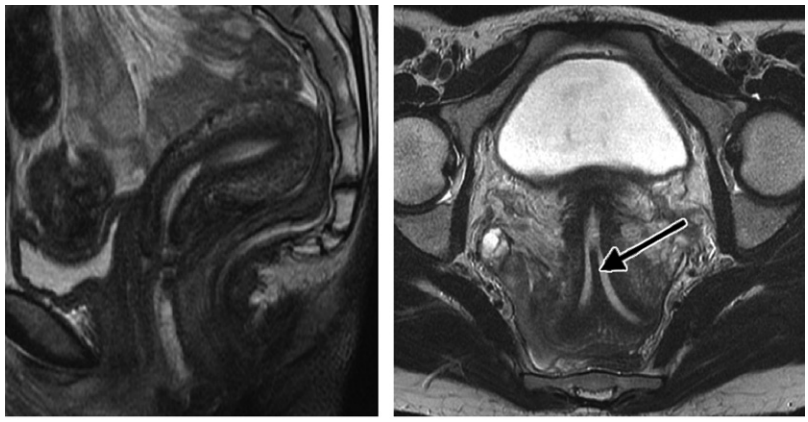

a. b.

Figure 9. Müllerian duct anomalies identified at transvaginal US in a 32-year-old woman. Sagittal **(a)** and axial **(b)** FSE T2-weighted MR images show a septate uterus (arrow on **b**).

Table 5: Previously Published Abbreviated MRI Protocols

Study	Indication	Contrast Agent	Acquisition Time (min)
Marks et al (38)	HCC surveillance	Gadoxetic acid	<10
Besa et al (39)	HCC screening	Gadoxetic acid	<10
Tillman et al (31)	HCC screening	Gadoxetic acid	<10
Lee et al (40)	HCC screening	Extracellular gadolinium-based contrast agent	<10
Cunha et al (45)	Nonalcoholic fatty liver disease surveillance	None	7
Stanzione et al (60)	Prostate cancer detection	None	≈17
Kuhl et al (61)	Prostate cancer detection	None	<9
Weiss et al (30)	Prostate cancer detection	None	5

Note.—Numbers in parentheses are reference citations.

Conclusion

Abbreviated MRI protocols are faster and may represent a lower-cost alternative to the standard MRI protocols. The reported results have shown similar performance for the abbreviated MRI protocol and the standard MRI protocol to detect and characterize lesions in the abdomen and pelvis. Table 5 summarizes previously published abbreviated MRI protocols (30,31,38–40,45,60,61).

Additional applications in the body present further opportunities for exploring abbreviated MRI protocols. However, prospective studies in larger cohorts are necessary to validate and confirm the robustness of such protocols, as well as to establish real cost savings, before their more widespread adoption in clinical practice.

***Disclosures of Conflicts of Interest.*—B.T.** *Activities related to the present article:* institutional grant from Bayer Healthcare. *Activities not related to the present article:* institutional grant from Guerbet. *Other activities:* disclosed no relevant relationships. **D.V.S.** *Activities related to the present article:* institutional grant from Bayer Healthcare. *Activities not related to the present article:* consultant for GE Healthcare; institutional grant from GE Healthcare; royalties from Elsevier. *Other activities:* disclosed no relevant relationships.

References

1. Rosenkrantz AB, Padhani AR, Chenevert TL, et al. Body diffusion kurtosis imaging: basic principles, applications, and considerations for clinical practice. J Magn Reson Imaging 2015;42(5):1190–1202.
2. Cheng HL, Stikov N, Ghugre NR, Wright GA. Practical medical applications of quantitative MR relaxometry. J Magn Reson Imaging 2012;36(4):805–824.
3. Bellomo G, Marcocci F, Bianchini D, et al. MR spectroscopy in prostate cancer: new algorithms to optimize metabolite quantification. PLoS One 2016;11(11):e0165730. https://doi.org/10.1371/journal.pone.0165730. Published November 10, 2016.
4. Erturk MA, Bottomley PA, El-Sharkawy AM. Denoising MRI using spectral subtraction. IEEE Trans Biomed Eng 2013;60(6):1556–1562.
5. Bardes CL. Defining "patient-centered medicine." N Engl J Med 2012;366(9):782–783.
6. O'Brien JJ, Stormann J, Roche K, et al. Optimizing MRI logistics: focused process improvements can increase throughput in an academic radiology department. AJR Am J Roentgenol 2017;208(2):W38–W44.

7. Beker K, Garces-Descovich A, Mangosing J, Cabral-Goncalves I, Hallett D, Mortele KJ. Optimizing MRI logistics: prospective analysis of performance, efficiency, and patient throughput. AJR Am J Roentgenol 2017;209(4):836–844.
8. Recht M, Macari M, Lawson K, et al. Impacting key performance indicators in an academic MR imaging department through process improvement. J Am Coll Radiol 2013;10(3):202–206.
9. Tokur S, Lederle K, Terris DD, et al. Process analysis to reduce MRI access time at a German university hospital. Int J Qual Health Care 2012;24(1):95–99.
10. Pirasteh A, VanDyke M, Bolton-Ronacher J, et al. Implementation of an online screening and check-in process to optimize patient workflow before outpatient MRI studies. J Am Coll Radiol 2016;13(8):956.e5–959.e5. https://www.jacr.org/article/S1546-1440(15)01214-4/fulltext. Published January 16, 2016.
11. Roth CJ, Boll DT, Wall LK, Merkle EM. Evaluation of MRI acquisition workflow with lean six sigma method: case study of liver and knee examinations. AJR Am J Roentgenol 2010;195(2):W150–W156.
12. Tsao J, Kozerke S. MRI temporal acceleration techniques. J Magn Reson Imaging 2012;36(3):543–560.
13. Hamilton J, Franson D, Seiberlich N. Recent advances in parallel imaging for MRI. Prog Nucl Magn Reson Spectrosc 2017;101:71–95.
14. Bauer S, Markl M, Honal M, Jung BA. The effect of reconstruction and acquisition parameters for GRAPPA-based parallel imaging on the image quality. Magn Reson Med 2011;66(2):402–409.
15. Chen Y, Li J, Qu X, et al. Partial Fourier transform reconstruction for single-shot MRI with linear frequency-swept excitation. Magn Reson Med 2013;69(5):1326–1336.
16. Zhang Z, Frydman L. Partial Fourier techniques in single-shot cross-term spatiotemporal encoded MRI. Magn Reson Med 2018;79(3):1506–1514.
17. Zhou R, Huang W, Yang Y, et al. Simple motion correction strategy reduces respiratory-induced motion artifacts for k-t accelerated and compressed-sensing cardiovascular magnetic resonance perfusion imaging. J Cardiovasc Magn Reson 2018;20(1):6. https://doi.org/10.1186/s12968-018-0427-1. Published February 1, 2018. [Published correction appears in J Cardiovasc Magn Reson 2018;20(1):23.]
18. Jung H, Ye JC, Kim EY. Improved k-t BLAST and k-t SENSE using FOCUSS. Phys Med Biol 2007;52(11):3201–3226.
19. Liang S, Dresselaers T, Louchami K, Zhu C, Liu Y, Himmelreich U. Comparison of different compressed sensing algorithms for low SNR ^{19}F MRI applications: imaging of transplanted pancreatic islets and cells labeled with perfluorocarbons. NMR Biomed 2017;30(11):e3776. https://onlinelibrary.wiley.com/doi/abs/10.1002/nbm.3776. Published November 23, 2017.
20. Chen L, Huang J, Zhang T, Li J, Cai C, Cai S. Variable density sampling and non-Cartesian super-resolved reconstruction for spatiotemporally encoded single-shot MRI. J Magn Reson 2016;272:1–9.
21. Kaltenbach B, Bucher AM, Wichmann JL, et al. Dynamic liver magnetic resonance imaging in free-breathing: feasibility of a Cartesian T1-weighted acquisition technique with compressed sensing and additional self-navigation signal for hard-gated and motion-resolved reconstruction. Invest Radiol 2017;52(11):708–714.
22. Teruel JR, Kuperman JM, Dale AM, White NS. High temporal resolution motion estimation using a self-navigated simultaneous multi-slice echo planar imaging acquisition. J Magn Reson Imaging 2018;48(3):780–787.
23. Koh DM, Collins DJ. Diffusion-weighted MRI in the body: applications and challenges in oncology. AJR Am J Roentgenol 2007;188(6):1622–1635.
24. Rosenkrantz AB, Oei M, Babb JS, Niver BE, Taouli B. Diffusion-weighted imaging of the abdomen at 3.0 Tesla: image quality and apparent diffusion coefficient reproducibility compared with 1.5 Tesla. J Magn Reson Imaging 2011;33(1):128–135.
25. Taron J, Johannink J, Bitzer M, Nikolaou K, Notohamiprodjo M, Hoffmann R. Added value of diffusion-weighted imaging in hepatic tumors and its impact on patient management. Cancer Imaging 2018;18(1):10. https://doi.org/10.1186/s40644-018-0140-1. Published March 7, 2018.
26. Boss A, Barth B, Filli L, et al. Simultaneous multi-slice echo planar diffusion weighted imaging of the liver and the pancreas: optimization of signal-to-noise ratio and acquisition time and application to intravoxel incoherent motion analysis. Eur J Radiol 2016;85(11):1948–1955.
27. Shankar S, Kalra N, Bhatia A, et al. Role of diffusion weighted imaging (DWI) for hepatocellular carcinoma (HCC) detection and its grading on 3T MRI: a prospective study. J Clin Exp Hepatol 2016;6(4):303–310.
28. Parikh T, Drew SJ, Lee VS, et al. Focal liver lesion detection and characterization with diffusion-weighted MR imaging: comparison with standard breath-hold T2-weighted imaging. Radiology 2008;246(3):812–822.
29. Proscia N, Jaffe TA, Neville AM, Wang CL, Dale BM, Merkle EM. MRI of the pelvis in women: 3D versus 2D T2-weighted technique. AJR Am J Roentgenol 2010;195(1):254–259.
30. Weiss J, Martirosian P, Notohamiprodjo M, et al. Implementation of a 5-minute magnetic resonance imaging screening protocol for prostate cancer in men with elevated prostate-specific antigen before biopsy. Invest Radiol 2018;53(3):186–190.
31. Tillman BG, Gorman JD, Hru JM, et al. Diagnostic per-lesion performance of a simulated gadoxetate disodium-enhanced abbreviated MRI protocol for hepatocellular carcinoma screening. Clin Radiol 2018;73(5):485–493.
32. Oldrini G, Derraz I, Salleron J, Marchal F, Henrot P. Impact of an abbreviated protocol for breast MRI in diagnostic accuracy. Diagn Interv Radiol 2018;24(1):12–16.
33. Heimbach JK, Kulik LM, Finn RS, et al. AASLD guidelines for the treatment of hepatocellular carcinoma. Hepatology 2018;67(1):358–380.
34. Zhang BH, Yang BH, Tang ZY. Randomized controlled trial of screening for hepatocellular carcinoma. J Cancer Res Clin Oncol 2004;130(7):417–422.
35. Colli A, Fraquelli M, Casazza G, et al. Accuracy of ultrasonography, spiral CT, magnetic resonance, and alpha-fetoprotein in diagnosing hepatocellular carcinoma: a systematic review. Am J Gastroenterol 2006;101(3):513–523.
36. Singal A, Volk ML, Waljee A, et al. Meta-analysis: surveillance with ultrasound for early-stage hepatocellular carcinoma in patients with cirrhosis. Aliment Pharmacol Ther 2009;30(1):37–47.
37. Yu NC, Chaudhari V, Raman SS, et al. CT and MRI improve detection of hepatocellular carcinoma, compared with ultrasound alone, in patients with cirrhosis. Clin Gastroenterol Hepatol 2011;9(2):161–167.
38. Marks RM, Ryan A, Heba ER, et al. Diagnostic per-patient accuracy of an abbreviated hepatobiliary phase gadoxetic acid–enhanced MRI for hepatocellular carcinoma surveillance. AJR Am J Roentgenol 2015;204(3):527–535.
39. Besa C, Lewis S, Pandharipande PV, et al. Hepatocellular carcinoma detection: diagnostic performance of a simulated abbreviated MRI protocol combining diffusion-weighted and T1-weighted imaging at the delayed phase post gadoxetic acid. Abdom Radiol (NY) 2017;42(1):179–190. [Published correction appears in Abdom Radiol (NY) 2018;43(3):760.]
40. Lee JY, Huo EJ, Weinstein S, et al. Evaluation of an abbreviated screening MRI protocol for patients at risk for hepatocellular carcinoma. Abdom Radiol (NY) 2018;43(7):1627–1633.
41. Niekel MC, Bipat S, Stoker J. Diagnostic imaging of colorectal liver metastases with CT, MR imaging, FDG PET, and/or FDG PET/CT: a meta-analysis of prospective studies including patients who have not previously undergone treatment. Radiology 2010;257(3):674–684.
42. Barabasch A, Distelmaier M, Kraemer NA, Bruners P, Kuhl CK. Abbreviated liver-MRI vs full protocol liver-MRI including hepatobiliary phase imaging to screen liver metastases in patients with solid tumors: preliminary results [abstr]. In: Radiological Society of North America scientific assembly and annual meeting program [book online]. Oak Brook, Ill: Radiological Society of North America, 2017. http://archive.rsna.org/2017/17018579.html. Accessed March 12, 2018.

43. Canellas R, Kilcoyne A, Sahani DV. Diagnostic performance of an abbreviated gadoxetic acid-enhanced MRI protocol for colorectal cancer liver metastases surveillance [abstr]. In: Radiological Society of North America scientific assembly and annual meeting program [book online]. Oak Brook, Ill: Radiological Society of North America, 2017. http://archive.rsna.org/2017/17017647.html. Accessed March 12, 2018.
44. Yin M, Glaser KJ, Talwalkar JA, Chen J, Manduca A, Ehman RL. Hepatic MR elastography: clinical performance in a series of 1377 consecutive examinations. Radiology 2016;278(1):114–124.
45. Cunha GM, Villela-Nogueira CA, Bergman A, Lobo Lopes FPP. Abbreviated mpMRI protocol for diffuse liver disease: a practical approach for evaluation and follow-up of NAFLD. Abdom Radiol (NY) 2018;43(9):2340–2350.
46. Lee KS, Sekhar A, Rofsky NM, Pedrosa I. Prevalence of incidental pancreatic cysts in the adult population on MR imaging. Am J Gastroenterol 2010;105(9):2079–2084.
47. Pinho DF, Rofsky NM, Pedrosa I. Incidental pancreatic cysts: role of magnetic resonance imaging. Top Magn Reson Imaging 2014;23(2):117–128.
48. Macari M, Lee T, Kim S, et al. Is gadolinium necessary for MRI follow-up evaluation of cystic lesions in the pancreas? preliminary results. AJR Am J Roentgenol 2009;192(1):159–164.
49. Nougaret S, Reinhold C, Chong J, et al. Incidental pancreatic cysts: natural history and diagnostic accuracy of a limited serial pancreatic cyst MRI protocol. Eur Radiol 2014;24(5):1020–1029.
50. Megibow AJ, Baker ME, Morgan DE, et al. Management of incidental pancreatic cysts: a white paper of the ACR Incidental Findings Committee. J Am Coll Radiol 2017;14(7):911–923.
51. Pedrosa I. A 10-min MRI protocol for follow up incidental cystic pancreatic lesions [abstr]. In: Radiological Society of North America scientific assembly and annual meeting program [book online]. Oak Brook, Ill: Radiological Society of North America, 2017. http://archive.rsna.org/2017/17001338.html. Accessed March 12, 2018.
52. Gardner TB, Glass LM, Smith KD, et al. Pancreatic cyst prevalence and the risk of mucin-producing adenocarcinoma in US adults. Am J Gastroenterol 2013;108(10):1546–1550.
53. Young WF Jr. Clinical practice: the incidentally discovered adrenal mass. N Engl J Med 2007;356(6):601–610.
54. Sahdev A. Recommendations for the management of adrenal incidentalomas: what is pertinent for radiologists? Br J Radiol 2017;90(1072):20160627. https://www.birpublications.org/doi/pdf/10.1259/bjr.20160627. Published March 20, 2017.
55. Paterson C, Yew-Fung C, Sweeney C, Szewczyk-Bieda M, Lang S, Nabi G. Predictors of growth kinetics and outcomes in small renal masses (SRM ≤4 cm in size): Tayside Active Surveillance Cohort (TASC) study. Eur J Surg Oncol 2017;43(8):1589–1597.
56. Nayyar M, Cheng P, Desai B, et al. Active surveillance of small renal masses: a review on the role of imaging with a focus on growth rate. J Comput Assist Tomogr 2016;40(4):517–523.
57. Hoeks CM, Barentsz JO, Hambrock T, et al. Prostate cancer: multiparametric MR imaging for detection, localization, and staging. Radiology 2011;261(1):46–66.
58. Rosenkrantz AB, Hemingway J, Hughes DR, Duszak R Jr, Allen B Jr, Weinreb JC. Evolving use of prebiopsy prostate magnetic resonance imaging in the Medicare population. J Urol 2018;200(1):89–94.
59. Polanec SH, Lazar M, Wengert GJ, et al. 3D T2-weighted imaging to shorten multiparametric prostate MRI protocols. Eur Radiol 2018;28(4):1634–1641.
60. Stanzione A, Imbriaco M, Cocozza S, et al. Biparametric 3T magnetic resonance imaging for prostatic cancer detection in a biopsy-naïve patient population: a further improvement of PI-RADS v2? Eur J Radiol 2016;85(12):2269–2274. [Published correction appears in Eur J Radiol 2017;87:125.]
61. Kuhl CK, Bruhn R, Krämer N, Nebelung S, Heidenreich A, Schrading S. Abbreviated biparametric prostate MR imaging in men with elevated prostate-specific antigen. Radiology 2017;285(2):493–505.
62. Greer MD, Shih JH, Lay N, et al. Validation of the dominant sequence paradigm and role of dynamic contrast-enhanced imaging in PI-RADS version 2. Radiology 2017;285(3):859–869.
63. Partridge EE, Greenlee RT, Riley TL, et al. Assessing the risk of ovarian malignancy in asymptomatic women with abnormal CA 125 and transvaginal ultrasound scans in the prostate, lung, colorectal, and ovarian screening trial. Obstet Gynecol 2013;121(1):25–31.
64. Lai T, Kessel B, Ahn HJ, Terada KY. Ovarian cancer screening in menopausal females with a family history of breast or ovarian cancer. J Gynecol Oncol 2016;27(4):e41. https://www.ejgo.org/Synapse/Data/PDFData/1114JGO/jgo-27-e41.pdf. Published April 6, 2016.
65. Sala E, Wakely S, Senior E, Lomas D. MRI of malignant neoplasms of the uterine corpus and cervix. AJR Am J Roentgenol 2007;188(6):1577–1587.
66. Sala E, Rockall AG, Freeman SJ, Mitchell DG, Reinhold C. The added role of MR imaging in treatment stratification of patients with gynecologic malignancies: what the radiologist needs to know. Radiology 2013;266(3):717–740.
67. Park JJ, Kim CK, Park SY, Park BK. Parametrial invasion in cervical cancer: fused T2-weighted imaging and high-*b*-value diffusion-weighted imaging with background body signal suppression at 3 T. Radiology 2015;274(3):734–741.
68. Qu JR, Qin L, Li X, et al. Predicting parametrial invasion in cervical carcinoma (stages IB1, IB2, and IIA): diagnostic accuracy of T2-weighted imaging combined with DWI at 3 T. AJR Am J Roentgenol 2018;210(3):677–684.
69. Deng L, Wang QP, Chen X, Duan XY, Wang W, Guo YM. The combination of diffusion- and T2-weighted imaging in predicting deep myometrial invasion of endometrial cancer: a systematic review and meta-analysis. J Comput Assist Tomogr 2015;39(5):661–673.
70. Nougaret S, Reinhold C, Alsharif SS, et al. Endometrial cancer: combined MR volumetry and diffusion-weighted imaging for assessment of myometrial and lymphovascular invasion and tumor grade. Radiology 2015;276(3):797–808.
71. Graupera B, Pascual MA, Hereter L, et al. Accuracy of three-dimensional ultrasound compared with magnetic resonance imaging in diagnosis of müllerian duct anomalies using ESHRE-ESGE consensus on the classification of congenital anomalies of the female genital tract. Ultrasound Obstet Gynecol 2015;46(5):616–622.